arXiv:1608.05028v2 [astro-ph.HE] 22 Dec 2016

The History of GRB Outflows: Ejection Lorentz Factor and Radiation Location of X-ray Flares

Hui-Jun Mu [1,2], Da-Bin Lin[1,2], Shao-Qiang Xi [1,3], Ting-Ting Lin[1,2], Yuan-Zhu Wang[1,2],Yun-Feng Liang[4], Lian-Zhong Lü[1,2], Jin Zhang[5], and En-Wei Liang [1,2,5]

ABSTRACT

We present time-resolved spectral analysis of the steep decay segments of 29 bright X-ray flares of gamma-ray bursts (GRBs) observed with the *Swift*/X-ray telescope, and model their lightcurves and spectral index evolution behaviors with the curvature effect model. Our results show that the observed rapid flux decay and strong spectral index evolution with time can be well fit with this model, and the derived characteristic timescales (t_c) are in the range of $33 \sim 264$ seconds. Using an empirical relation between the peak luminosity and the Lorentz factor derived from the prompt gamma-rays, we estimate the Lorentz factors of the flares ($\Gamma_{\rm X}$). We obtain $\Gamma_{\rm X} = 17 \sim 87$ with a median value of 52, which is smaller than the initial Lorentz factors of prompt gamma-ray fireballs. With the derived t_c and $\Gamma_{\rm X}$, we constrain the radiating regions of 13 X-ray flares, yielding $R_{\rm X} = (0.2 \sim 1.1) \times 10^{16}$ cm, which are smaller than the radii of the afterglow fireballs at the peak times of the flares. A long evolution feature from prompt gamma-ray phase to the X-ray epoch is found by incorporating our results with a sample of GRBs whose initial Lorentz factors are available in literatures, i.e., $\Gamma \propto [t_p/(1+z)]^{-0.69\pm0.06}$. These results may shed lights on the long term evolution of GRB central engines.

Subject headings: gamma-ray burst: general

[1]GXU-NAOC Center for Astrophysics and Space Sciences, Department of Physics, Guangxi University, Nanning 530004, China;lindabin@gxu.edu.cn, lew@gxu.edu.cn

[2]Guangxi Key Laboratory for the Relativistic Astrophysics, Nanning 530004, China

[3]Department of Mathematics and Physics, Officers College of CAPF, Chengdu, 610213,China

[4]Purple Mountain Observatory, Chinese Academy of Sciences, Nanjing 210008, China

[5]National Astronomical Observatories, Chinese Academy of Sciences, Beijing 100012, China

1. Introduction

Gamma-ray bursts (GRBs) are the most extreme explosive events in the universe. The duration of the prompt gamma-rays ranges from milliseconds to thousands of seconds (Kouveliotou et al. 1993), and afterglows following the prompt gamma-ray phase were found in the X-ray, optical, and radio bands. It is generally believed that the prompt gamma-rays are from internal shocks of collisions among fireball shells and the afterglows are from external shocks when the fireball shells propagate into the circum medium (e.g., Mészáros & Rees 1993; Rees & Mészáros 1994; Mészáros & Rees 1997; Piran 2004; Zhang & Mészáros 2004). With promptly slewing capacity, the X-ray telescope (XRT) onboard the Swift mission observed erratic flares during the prompt gamma-ray phase and even up to several days post the GRB trigger (e.g., Burrows et al. 2005; Zhang et al. 2006; Nousek et al. 2006; O'Brien et al. 2006; Falcone et al. 2006; Falcone et al. 2007; Chincarini et al. 2007; Chincarini et al. 2010). These flares are found to be internal origin and they sinal the restart of the GRB central engine after the prompt gamma-rays (e.g., Burrows et al. 2005; Fan & Wei 2005; Zhang et al. 2006; Dai et al. 2006; Proga & Zhang 2006; Perna et al. 2006; Romano et al. 2006; Liang et al. 2006; Wu et al. 2006 ; Margutti et al. 2010; Maxham & Zhang 2009)[1]. Taking these flares into account, the duration of the GRB central engines are much longer than the duration of the prompt gamma-rays (Qin et al. 2013; Virgili et al. 2013; Levan et al. 2014; Zhang et al. 2014).

X-ray flares are one of the most powerful diagnostic tools for the GRB central engines, especially their long term evolution behaviors (e.g., Dai et al. 2006). The radiation region and the bulk Lorentz factor of fireballs for early prompt gamma-rays and late X-ray flares are of great theoretical interest. Although it is still quite uncertain, the radiation region of the prompt gamma-rays is generally believed to be around $10^{13} - 10^{15}$ cm and the fireballs are ultra-relativistic with a Lorentz factor (Γ_γ) being greater than 100 (e.g., Mészáros & Rees 1993; Rees & Mészáros 1994; Piran 2004; Zhang & Mészáros 2004). With the deceleration timescale observed in the afterglow lightcurves, the derived Γ_γ values are usually in the range from 100 to 1000 (Sari & Piran 1999; Kobayashi & Zhang 2007; Molinari et al. 2007), and they are tightly correlated with the isotropic gamma-ray energy ($E_{\rm iso}$) and luminosity ($L_{\rm iso}$) of the prompt gamma-rays ($\Gamma_\gamma - E_{\gamma,\rm iso}$ relation; Liang et al. 2010, 2013; Lü et al. 2012). Furthermore, Liang et al. (2015) discovered a tight $L_{\rm iso} - E_{\rm p,z} - \Gamma_\gamma$ relation, where $E_{\rm p,z}$ is the peak energy of the νf_ν spectrum of prompt gamma-rays in the burst frame. The value of Γ_γ may be also estimated with the high energy cutoff in the prompt gamma-ray spectrum based on "compactness" argument (Fenimore et al. 1993; Woods & Loeb

[1]Alternatively, Hascoet et al. (2015) suggested that X-ray flares may be produced by the long-lived reverse shock when it crosses the tail of the GRB ejecta. Although this scenario may produce the observed temporal feature of the flares, it seems to be difficult in explaining the observed strong spectral variation in the flares (e.g., Butler& Kocevski 2007).

1995; Baring & Harding 1997; Lithwick & Sari 2001; Gupta & Zhang 2008). More recently, Tang et al. (2014) systematically searched for such a high energy spectral cutoff/break in GRBs observed with *Fermi*/LAT. They estimated the Γ_γ values for 9 GRBs with the observed cutoffs by assuming that these cutoffs are caused by pair-production absorption within the sources. They found Γ_γ values are also larger than 100, and confirmed the $\Gamma_\gamma - E_{\gamma,\rm iso}$ relation. For late X-ray flares, the Lorentz factor ($\Gamma_{\rm X}$) was suggested to be smaller than that of the fireballs producing the prompt gamma-rays (e.g., Fan & Wei 2005; c.f. Burrows et al. 2005). With the thermal emission observed in X-ray flares, Peng et al. (2014) obtained $\Gamma_{\rm X}$ being around $60 \sim 150$. The curvature effect, which is due to the observer receiving the progressively delayed emission from higher latitudes (Fenimore et al. 1996;Kumar & Panaitescu 2000; Qin 2002; Dermer 2004; Uhm & Zhang 2014), may present tight constraint on the emission region and its Lorentz factor of X-ray flares (e.g., Zhang et al. 2006; Lazzati & Begelman 2006). Jin et al. (2010) estimated $\Gamma_{\rm X}$ with both the thermal emission in the flares and the curvature effect on the decay phases of the flares and found that $\Gamma_{\rm X}$ ranges around tens. The radiation regions of the X-ray flares ($R_{\rm X}$) are even more poorly known. Troja et al. (2014) analyzed the flares with peaking time at $100 \sim 300$ seconds post the GRB trigger. They showed that $R_{\rm X} = 10^{13} - 10^{14}$ cm with $\Gamma_{\rm X} > 50$ in the framework of internal shock model if the variability timescale is significantly shorter than the observed flare duration.

As mentioned above, the origin of the flares may be the same as that of prompt gamma-rays. One may estimate $\Gamma_{\rm X}$ by assuming that the flares follow the same $\Gamma_\gamma - L_{\rm iso}$ relation. Further more, it is believed that the steep decay observed in the X-ray flares is due to the curvature effect (Fan & Wei 2005; Dyks et al. 2005; Liang et al. 2006; Zhang et al. 2006; Panaitescu et al. 2006; Wu et al. 2006; Zhang et al. 2007; Zhang et al. 2009; Qin 2008; c.f., Hascoët et al. 2015). This paper dedicates to study $\Gamma_{\rm X}$ and $R_{\rm X}$ of X-ray flares based the $\Gamma_\gamma - L_{\gamma,\rm iso}$ relation and the curvature effect on the X-ray flare tails. We select a sample of 29 bright X-ray flares (§2) and fit the lightcurve and the evolving spectral index during the steep decay phases of these X-ray flares based on our curvature effect model (§3). We constrain $R_{\rm X}$ and $\Gamma_{\rm X}$ values based on our fitting results in §4. Conclusions and discussions are presented in §5. Notation $Q_n = Q/10^n$ in cgs units are adopted.

2. Sample and Data Analysis

We present an extensive temporal and spectral analysis for the X-ray flares observed with Swift/XRT during 10 observation years (from 2005 to 2014). The XRT lightcurve data are downloaded from the website *http://www.swift.ac.uk/* (Evans et al. 2009) and fitted with a multi-component model composing of single power-law and broken power-law functions. This analysis focuses on the steep decay segments of the flares only. We obtain a sample of 29 X-ray flares which satisfy the following criteria. First, they are bright with $F_p/F_u > 10$, where F_p and F_u are the peak flux of the

flares and the flux of the underlying afterglow component. Second, the decay segments of the flares clearly decline without superimposing other flares or significant fluctuations. The time-resolved spectral analysis for the steep decay segments of flares are made with an absorbed single power-law model, i.e., $N(E) = N_0 * wabs * zwabs * E^{-(\beta+1)}$ and $N(E) = N_0 * wabs * wabs * E^{-(\beta+1)}$ with known redshift and unknown redshift, where "wabs" and "zwabs" are the photoelectric absorbtion of both our Galaxy and GRB host galaxies, respectively. Since the gas-to-dust ratio of GRB host galaxies are very uncertain (Starling et al. 2007; Li et al. 2008; Schady et al. 2012), we ignore the dust scattering effect in calculation of $N_{\rm H}$ values and adopt the same absorbtion model as that of our Galaxy for the GRB host galaxies at redshift z. We derive the $N_{\rm H}$ value of the host galaxy from the X-ray afterglow data for a given burst and make the time-resolved spectral analysis by keeping this value as a constant. The spectral analysis results are reported in Table 1. The evolution of the spectral index with time is also shown in Figure 1, where the peak time of the X-ray flare is set as the beginning time ($t = 0$) of the steep decay segment for our analysis.

3. Modeling the Steep Decay Segments in the Curvature Effect Scenario

As mentioned in §1, the steep decaying segment of the flares with a slope $\alpha = 2 + \beta$ would be due to the curvature effect, where β is the power-law index of the radiation spectrum (e.g., Fenimore et al. 1996; Kumar & Panaitescu 2000; Dermer 2004; Liang et al. 2006; Zhang et al. 2007). The curvature effect is a combination of the time delay and the Doppler shifting of the intrinsic spectrum for high latitude emission with respect to that in the light of sight. The time delay of photons from radius $R_{\rm X}$ and latitude angle θ with respect to those from $R_{\rm X}$ and $\theta = 0$ is given by

$$t = (1 + z)(R_{\rm X}/c)(1 - \cos\theta), \tag{1}$$

where z is the redshift of the studied source and c is the speed of light. For a relativistic moving jet with a Lorentz factor $\Gamma_{\rm X}$, the comoving emission frequency ν' is boosted to $\nu = D\nu'$ in the observers frame, where D is the Doppler factor described as

$$D = [\Gamma_{\rm X}(1 - \beta_{\rm jet}\cos\theta)]^{-1} \approx \left[\frac{1}{2\Gamma_{\rm X}} + \Gamma_{\rm X}(1 - \cos\theta)\right]^{-1} = \frac{2\Gamma_{\rm X}}{(1 + t/t_c)} \tag{2}$$

where $\beta_{\rm jet}c$ is the jet velocity, and t_c is a characteristic timescale of the curvature effect, which is

$$t_c = \frac{R_{\rm X}(1 + z)}{2\Gamma_{\rm X}^2 c}. \tag{3}$$

In case of a single power-law radiation spectrum, the observed spectral index would do not evolve with time (e.g., Fenimore et al. 1996; Dermer et al. 2004; Liang et al. 2006). The observed significant spectral softening as shown in Figure 1 would be due to the curvature effect on a curved

radiation spectrum (e.g., Zhang et al. 2007; 2009). Following Zhang et al. (2009), we fit the lightcurves and the spectral evolution features of the steep decay segments in our sample in the curvature effect scenario. We take the intrinsic radiation spectrum as a cut-off power-law parameterized as (Zhang et al. 2009) [2],

$$N'(E') = N'_0 \left(\frac{E'}{1\mathrm{keV}}\right)^{-\hat{\beta}} \exp\left[-\left(\frac{E'}{E'_c}\right)^{\kappa}\right], \tag{4}$$

where $\hat{\beta}$ is the photon index and E'_c is the cut-off energy. Parameter κ measures the steepness of the spectrum at $E' > E'_c$, as shown in Figure 2. We normally take $\kappa = 1$ in this analysis. Zhang et al. (2009) showed that such an intrinsic radiation spectrum can present the observed spectral index and flux evolution behaviors of GRB 050814 with the curvature effect model. The observed flux at photon energy E then can be calculated with $F_E \propto D^2 E' N'(E')$, i.e.,

$$F_E(t) = F_{E,0} \left(1 + \frac{t}{t_c}\right)^{-1-\hat{\beta}} \exp\left[-\frac{E}{E_{c,0}}\left(1 + \frac{t}{t_c}\right)\right] \left(\frac{E}{1\mathrm{keV}}\right)^{-\hat{\beta}+1}, \tag{5}$$

where $F_{E,0}$ and $E_{c,0} \equiv 2\Gamma_X E'_c$ are the observed on-axis flux and cut-off photon energy (corresponding to $t = 0$), respectively. The observed flux in the XRT band then can be given by

$$F_{\mathrm{XRT}}(t) = \int_{0.3\mathrm{keV}}^{10\mathrm{keV}} F_E dE. \tag{6}$$

We simply calculate the observed spectral index in the XRT band at t with

$$\beta(t) = -\frac{\log\left(F_{10\mathrm{keV}}(t)\right) - \log\left(F_{0.3\mathrm{keV}}(t)\right)}{\log\left(10\mathrm{keV}\right) - \log\left(0.3\mathrm{keV}\right)}. \tag{7}$$

We make jointed fits to the lightcurves and β evolution with Eqs. (6) and (7). The peak time of flares is set as the zero time $t = 0$ in these equations [3]. The goodness of our fits is evaluated with the total reduced χ^2 by weighting the data points between that in the lightcurves and in the spectral evolution. The total χ^2 value is given by $\chi^2 = \chi^2_{\mathrm{LC}} + \chi^2_{\beta}$, where subscripts "LC" and "β" indicate the lightcurves and the β evolution curves. We minimize χ^2 in our fits.

[2]The choice of this function was also due to the fact that the spectral evolution of some GRB tails can be fitted by such an empirical model (Campana et al. 2006; Zhang et al. 2007; Yonetoku et al. 2008).

[3]Note that our fits by setting t_0 as a free parameter may lead to unreasonable results being due to the degeneracy of t_c and t_0 in our model. Liang et al. (2006) showed that the t_0 values are in the rising segment of the corresponding pulses or flares. Since the flux of flares usually rapidly increase in the rising segment, we simply set the zero time of the flares at the peak times in this analysis.

Only 13 GRBs in our sample have redshift measurement. Our fit curves are displayed in Figure 1, and the model parameters, including $F_{\rm E0}$, $\hat{\beta}$, $E_{c,\,0}$, and t_c, are reported in Table 2. One can observed that our model can represent the observed flux decay and spectral index evolution in these flares. The t_c values range from 33 to 264 seconds, as shown in Figure 3.

4. The Lorentz Factor and Radiation Location of X-Ray Flares

As shown in Eq. (3), one may estimate $R_{\rm X}$ or $\Gamma_{\rm X}$ with the derived t_c if one of them is available by another way. By deriving $R_{\rm X}$ with a tentative jet break, Jin et al. (2010) got $\Gamma_{\rm X} = 22, 13$ for GRBs 050502B and 050724, respectively. Note that a tight $\Gamma_\gamma - E_{\gamma,\rm iso}$ or $\Gamma_\gamma - L_{\gamma,\rm iso}$ relations were found by Liang et al. (2010) and Lü et al. (2012)[4]. Assuming that the flares follow the $\Gamma_\gamma - L_{\gamma,\rm iso}$ relation, one can use this relation to estimate $\Gamma_{\rm X}$, then derive $R_{\rm X}$ with Eq. (3).

Lü et al. (2012) derived the $\Gamma_\gamma - L_{\gamma,\rm iso}$ relation by using the average luminosity of the prompt gamma-rays. Since burst durations depend on the energy band selected (e. g., Qin et al. 2013), it is difficult to accurately measure the duration of flares. Therefore, we use the peak luminosity of the flares for our analysis. In addition, Lü et al. (2012) adopted the ordinary least-square regression method to obtain the regression line. For regression analysis, the fitting results depend on the specification of dependent and independent variables (Isobe et al. 1990). One may find discrepancy of the relations among variables by specifying different dependent variables for a given data set, especially when the data have large error bars or scatters. To avoid specifying independent and dependent variables in the best linear fits, we adopt the algorithm of the bisector of two ordinary least-squares to re-do the regression analysis. The derived $\Gamma_\gamma - L_{\gamma,\rm p}$ relation is

$$\log \Gamma_\gamma = (2.27 \pm 0.04) + (0.34 \pm 0.03) \log L_{\gamma,\rm p,52}. \quad (8)$$

It is roughly consistent with that reported in Lü et al. (2012). We check if X-ray flares follow this relation with a flare observed in GRB 050724. With its $L_{\rm X,p} = 9.2 \times 10^{47}$ erg/s, we get $\Gamma = 7.9$, which is comparable to that reported by Jin et al. (2010), i.e., $\Gamma_{\rm X} = 13$. We thus use this correlation to estimate the $\Gamma_{\rm X}$ with the peak luminosity of the flares for the 13 GRBs whose redshifts are available. Our results are reported in Table 3. One can find that $\Gamma_{\rm X} = 17 \sim 87$, with a median value of $\Gamma_{\rm X} = 52$. The derived $\Gamma_{\rm X}$ values are generally consistent with that reported in previous papers (e.g., Fan & Wei 2005; Falcone et al. 2006; Panaitescu 2006).

It is generally believed that X-ray flares are powered by the late activities of the GRB central

[4]Ghirlanda et al. (2012) used a different method to estimate the Γ_0 values. Their method applies the Blandford-CMckee (BM) self-similar deceleration solution (Blandford& McKee 1976) and extrapolates it backward to derive Γ_0. They derived a different slope of the $\Gamma_0 - L_{\gamma,\rm iso}$ relation.

engine. The derived $\Gamma_{\rm X}$ values in this analysis are systematically smaller than the Γ_0 values of the prompt gamma-rays as that reported in Liang et al. (2010, 2013) and Tang et al. (2014). In addition, with the thermal emission observed in the joint BAT and XRT spectra of 13 early flares, which are usually observed at the end of the prompt gamma-ray phase, Peng et al. (2014) derived the $\Gamma_{\rm X}$ values for these flares by assuming that the thermal emission is the photosphere emission of the GRB fireballs. They found that the Lorentz factors range between 50 and 150. They are also systematically larger than the $\Gamma_{\rm X}$ values of late flares in our analysis. To explore possible evolution feature of the Lorentz factor, we plot Γ as a function of t_p in the burst frame for prompt gamma-rays and X-ray flares in Figure 4 with samples from Liang et al. (2013), Peng et al. (2014), Troja et al. (2014), Tang et al. (2014), and Fan & Wei (2005), where the t_p of prompt gamma-rays is taken as the middle of burst duration. One can observe a trend that Γ values (both Γ_0 and $\Gamma_{\rm X}$) decay with time. The Spearman correlation analysis yields a correlation coefficient $r = 0.70$ and a chance probability $p < 10^{-4}$. This may illustrate a long term evolution feature of the GRB central engines (e.g., Lazzati et al. 2008). We derive the relation of Γ to $t_{\rm p}/(1+z)$ with the algorithm of the bisector of two ordinary least-squares, which yields $\Gamma = 10^{3.05\pm0.11} \times [t_p/(1+z)]^{-0.69\pm0.06}$.

With the derived $\Gamma_{\rm X}$, we calculate $R_{\rm X}$ values for the 13 GRBs with Eq. (8). The results are also reported in Table 3. It is found that $R_{\rm X} = 2.0 \times 10^{15} \sim 1.1 \times 10^{16}$ cm, with a median value of $R_{\rm X} = 6.5 \times 10^{15}$ cm. The radiation regions of the flares are within the regions of the prompt gamma-rays and afterglows. It was generally accepted that the locations of the prompt gamma-rays and afterglows are $\sim 10^{13}$ cm and 10^{17} cm (e.g., Zhang & Mészáros 2004) , respectively. Troja et al. (2014) analyzed the flares with peaking time at $100 \sim 300$ seconds post the GRB trigger. They found $R_{\rm X} \sim 10^{13} - 10^{14}$ cm with $\Gamma_{\rm X} > 50$ in the framework of internal shock models, if the variability timescale is significantly shorter than the observed flare duration. Their $R_{\rm X}$ values are consistent with that producing early prompt gamma-rays. However, as shown in Peng et al. (2014), the photosphere radii of the flares at the end of the prompt gamma-ray emission phase in their sample are usually 10^{13} cm. The internal shock regions of these flares should be beyond the photosphere radius, i.e., $R_{\rm X} \gtrsim 10^{13}$ cm. The $R_{\rm X}$ values for the late flares in this analysis are in the range of $2.0 \times 10^{15} \sim 1.1 \times 10^{16}$ cm, which is much larger than that of the prompt gamma-rays. We estimate the fireball radii of the afterglows at the flare epochs with $R_{\rm AG} = 1.1\times10^{17}{\rm cm}[(1+z)/2.0]^{-1/2}(E_{\rm k}/10^{52}{\rm erg})^{1/2}A_*^{-1/2}(t_p/1{\rm day})^{1/2}$ (Chevalier & Li 2000), where $E_{\rm k}$ is the kinetic energy of the fireballs and A_* is the wind parameter. We calculate $E_{\rm k}$ values with $E_{\rm k} = (1-\eta_\gamma)E_{\gamma,{\rm iso}}/\eta_\gamma$, where η_γ is the radiative efficiency of prompt emission and it is taken as 0.2 (Frail et al. 2001; Molinari et al. 2007; Liang et al. 2010). The wind parameter is set as $A_* = 1$. Figure 5 shows the comparison of $R_{\rm X}$ with $R_{\rm AG}$. We find that they are satisfied with $R_{\rm AG}/50 < R_{\rm X} < R_{\rm AG}$, indicating that the emission regions of the flares are in a broad range, but they are smaller than the radii of the fireballs for the afterglows. The narrow distribution of $R_{\rm X}$ of the flares in this analysis would be due to the sample selection effect since we select only late

flares in order to eliminate the contamination of adjacent flares.

5. Conclusions and Discussion

We have fit the lightcurves and the spectral evolution during the steep decay segment in 29 late X-ray flares with the curvature effect model. We show that this model may well represent both the spectral and temporal behaviors in the steep decay segments. The derived characteristic timescale t_c are in the range of $33 \sim 264$ seconds, spreading about one order of magnitude. Using the relation between the peak luminosity and the Lorentz factor derived from the prompt gamma-rays, we estimate the Lorentz factors of the flares and find $\Gamma_{\rm X} = 17 \sim 87$ with a median value of 52. With the flares in our sample, together with samples collected from literature for prompt gamma-ray emission and early X-ray flares, we find a tentative correlation between the Lorentz factor and the peak time of the flares (or the middle time of the prompt gamma-ray duration), i.e., $\Gamma \propto [t_p/(1+z)]^{-0.69\pm0.06}$. With the derived t_c and $\Gamma_{\rm X}$, we constrain the radiating region as $R_{\rm X} = 2.0 \times 10^{15} \sim 1.1 \times 10^{16}$ cm, with a median value of 6.5×10^{15} cm. The radiation regions of the flares are within the regions of the prompt gamma-rays and afterglows, and the narrow distribution of $R_{\rm X}$ of the flares in this analysis would be due to the sample selection effect since we select only late flares in order to eliminate the contamination of adjacent flares.

The derived $\Gamma - t_{\rm p}$ anti-correlation indicates the decay of the Lorentz factor of ejecta. It may feature the long-term evolution of central engines. With the relation of $\Gamma \propto [t_p/(1+z)]^{-0.69\pm0.06}$ and Eq. (8), one can obtain $L_{\rm X,p} \propto [t_p/(1+z)]^{-2}$. Lazzati et al. (2008) derived a similar power-law index for the correlation between the mean luminosity and the peak time of the individual flares for 10 long GRBs that have multiple flares. They suggested that accretion onto a compact object could explain this feature. Statistics for bright flares gives $L \propto [t_{\rm p}/(1+z)]^{-1.9}$ (Chincarini et al. 2010). Margutti et al. (2011) found the average peak luminosity of the early flares ($30 < t_p < 1000$ seconds) decays as $L \propto t^{-2.7\pm0.1}$. They argued that this feature could be triggered by a rapid outward expansion of an accretion shock in the material feeding a convective disc in hyper-accreting black hole scenario. Note that the discrepancy of the derived power-law indices would be due to the sample selection.

Note that the luminosity $L_{\rm X,p}$ values of the flares in our work are calculated in the XRT band. They may be underestimated, especially for the early X-ray flares. It is well known that the GRB spectra are usually well fit with the Band function in a broad energy band (e.g., Zhang et al. 2011). As shown in Peng et al. (2014), some early X-ray flares are the soft extension of the gamma-ray pulses and the E_p values of their spectra are higher than the XRT band. Their X-ray luminosity values observed in the XRT band are only a small fraction of their bolometric luminosity. Looking at Table 1, one can observe $\beta < 1$ for some flares, indicating that their energy fluxes would go up

to a higher energy band. For those flares with $\beta > 1$, the luminosity observed in the XRT band could be a good representative of the bolometric luminosity, and the $\Gamma_{\rm X}$ values derived from Eq. (8) with $L_{\rm X,p}$ measured in the XRT band is only lower limits of Γ_X. Then, the true $\Gamma - t_{\rm p}$ relation would become shallower than that derived in this analysis. In addition, with spectral information of prompt gamma-rays collected from Butler et al. (2007), Ghirlanda et al. (2008),and Heussa et al. (2013), we also derive the luminosity at 10 keV ($L_{10\ \rm keV}$) for the GRBs reported in LV (2012) and checked whether it is still tightly correlated with Γ_0. We found that it is not. This is reasonable since $L_{10\ \rm keV}$ is only a very small fraction of the radiation luminosity. Although Γ_0 is tightly correlated with the bolometric luminosity, it is not necessary to be correlated with any selected mono-frequency luminosity. Therefore, in case of that the luminosity in the XRT band is not a good representative of the bolometric luminosity, the derived Γ_X with Eq. (8) may be quite uncertain.

The $R_{\rm X}$ values derived in this analysis are between the prompt gamma-ray and afterglow radiating regions. Since $\Gamma_{\rm X}$ may be underestimated as we mentioned above, the inferred $R_{\rm X}$ with Eq. (3) thus ma ybe also underestimated, which is somewhat compensated by the assumption that the flare decay timescale t_c is set by the curvature effect. It could be that t_c is dominated by something else, and the t_c reported here may overestimate the true curvature timescale. Recently, Uhm & Zhang (2015) found that the decay slope is steeper than the standard value from the curvature effect model if the jet is undergoing bulk acceleration when the emission ceases. They showed that the decay properties of flares demand that the emission region is undergoing significant bulk acceleration (seel also Jia et al. 2016). Therefore, the dynamical timescale and the magnetic field decay timescale would dominate the flare decay timescale and the t_c value may be smaller, hence the real $R_{\rm X}$ would be smaller than that reported in this analysis.

We acknowledge the use of the public data from the Swift data archive. We thank the anonymous referee for helpful suggestions to improve the paper. We also appreciate helpful discussion with Bing Zhang, Xue-Feng Wu, and Shu-Jin Hou. This work is supported by the National Basic Research Program of China (973 Program, grant No. 2014CB845800), the National Natural Science Foundation of China (Grant No. 11533003, 11403005, 11373036, 11163001), the Strategic Priority Research Program The Emergence of Cosmological Structures of the Chinese Academy of Sciences (grant XDB09000000), the Guangxi Science Foundation (Grant No. 2014GXNSFBA118004, 2013GXNSFFA019001), and the Project Sponsored by the Scientific Research Foundation of Guangxi University (Grant No. XJZ140331).

REFERENCES

Baring, M. G., & Harding, A. K. 1997, ApJ, 491, 663

Burrows, D. N., Romano, P., Falcone, A., et al. 2005, Science, 309, 1833

Butler, N. R., Kocevski, D., Bloom, J. S., & Curtis, J. L. 2007, ApJ, 671, 656

Butler, N. R., & Kocevski, D. 2007, ApJ, 668, 400

Chevalier, R. A., & Li, Z.-Y. 2000, ApJ, 536, 195

Blandford, R. D., & McKee, C. F. 1976, Physics of Fluids, 19, 1130

Chincarini, G., Mao, J., Margutti, R., et al. 2010, MNRAS, 406, 2113

Chincarini, G., Moretti, A., Romano, P., et al. 2007, ApJ, 671, 1903

Dai, Z. G., Wang, X. Y., Wu, X. F., & Zhang, B. 2006, Science, 311, 1127

Dermer, C. D. 2004, ApJ, 614, 284

Dyks, J., Zhang, B., & Fan, Y. Z. 2005, arXiv:astro-ph/0511699

Evans, P. A., Beardmore, A. P., Page, K. L., et al. 2009, MNRAS, 397, 1177

Falcone, A. D., Burrows, D. N., Lazzati, D., et al. 2006, ApJ, 641, 1010

Falcone, A. D., Morris, D., Racusin, J., et al. 2007, ApJ, 671, 1921

Fan, Y. Z., & Wei, D. M. 2005, MNRAS, 364, L42

Fenimore, E. E., Epstein, R. I., & Ho, C. 1993, A&AS, 97, 59

Fenimore, E. E., Madras, C. D., & Nayakshin, S. 1996, ApJ, 473, 998

Frail, D. A., Kulkarni, S. R., Sari, R., et al. 2001, ApJ, 562, L55

Ghirlanda, G., Nava, L., Ghisellini, G., Firmani, C., & Cabrera, J. I. 2008, MNRAS, 387, 319

Ghirlanda, G., Nava, L., Ghisellini, G., et al. 2012, MNRAS, 420, 483

Gupta, N., & Zhang, B. 2008, MNRAS, 384, L11

Hascoet, R., Beloborodov, A. M., Daigne, F., & Mochkovitch, R. 2015, arXiv:1503.08333

Heussaff, V., Atteia, J.-L., & Zolnierowski, Y. 2013, A&A, 557, A100

Jin, Z.-P., Fan, Y.-Z., & Wei, D.-M. 2010, ApJ, 724, 861

Kobayashi, S., & Zhang, B. 2007, ApJ, 655, 973

Kouveliotou, C., Meegan, C. A., Fishman, G. J., et al. 1993, ApJ, 413, L101

Kumar, P., & Panaitescu, A. 2000, ApJ, 541, L51

Lü, J., Zou, Y.-C., Lei, W.-H., et al. 2012, ApJ, 751, 49

Lazzati, D., & Begelman, M. C. 2006, ApJ, 641, 972

Lazzati, D., & Perna, R. 2007, MNRAS, 375, L46

Lazzati, D., Perna, R., & Begelman, M. C. 2008, MNRAS, 388, L15

Levan, A. J., Tanvir, N. R., Starling, R. L. C., et al. 2014, ApJ, 781, 13

Li, Y., Li, A., & Wei, D. M. 2008, ApJ, 678, 1136

Liang, E. W., Zhang, B., O'Brien, P. T., et al. 2006, ApJ, 646, 351

Liang, E.-W., Li, L., Gao, H., et al. 2013, ApJ, 774, 13

Liang, E.-W., Yi, S.-X., Zhang, J., et al. 2010, ApJ, 725, 2209

Liang, E.-W., Lin, T.-T., Lü, J., et al. 2015, ApJ, 813, 116

Lithwick, Y., & Sari, R. 2001, ApJ, 555, 540

Isobe, T., Feigelson, E. D., Akritas, M. G., & Babu, G. J. 1990, ApJ, 364, 104

Jia, L.-W., Uhm, Z. L., & Zhang, B. 2016, ApJS, 2016, 225, 17

Margutti, R., Guidorzi, C., Chincarini, G., et al. 2010, MNRAS, 406, 2149

Margutti, R., Bernardini, G., Barniol Duran, R., et al. 2011, MNRAS, 410, 1064

Maxham, A., & Zhang, B. 2009, ApJ, 707, 1623

Mészáros, P., & Rees, M. J. 1993, ApJ, 405, 278

Mészáros, P., & Rees, M. J. 1997, ApJ, 476, 232

Molinari, E., Vergani, S. D., Malesani, D., et al. 2007, A&A, 469, L13

Nousek, J. A., Kouveliotou, C., Grupe, D., et al. 2006, ApJ, 642, 389

Norris, J. P., Nemiroff, R. J., Bonnell, J. T., et al. 1996, ApJ, 459, 393

O'Brien, P. T., Willingale, R., Osborne, J., et al. 2006, ApJ, 647, 1213

Panaitescu, A. 2006, MNRAS, 367, L42

Peng, F.-K., Liang, E.-W., Wang, X.-Y., et al. 2014, ApJ, 795, 155

Perna, R., Armitage, P. J., & Zhang, B. 2006, ApJ, 636, L29

Piran, T. 2004, Reviews of Modern Physics, 76, 1143

Proga, D., & Zhang, B. 2006, MNRAS, 370, L61

Qin, Y.-P. 2002, A&A, 396, 705

Qin, Y.-P. 2008, ApJ, 683, 900

Qin, Y., Liang, E.-W., Liang, Y.-F., et al. 2013, ApJ, 763, 15

Rees, M. J., & Mészáros, P. 1994, ApJ, 430, L93

Romano, P., Moretti, A., Banat, P. L., et al. 2006, A&A, 450, 59

Sari, R., & Piran, T. 1999, ApJ, 520, 641

Schady, P., Dwelly, T., Page, M. J., et al. 2012, A&A, 537, AA15

Starling, R. L. C., Wijers, R. A. M. J., Wiersema, K., et al. 2007, ApJ, 661, 787

Tang, Q.-W., Peng, F.-K., Wang, X.-Y., & Tam, P.-H. T. 2014, arXiv:1412.3342

Troja, E., Piro, L., Vasileiou, V., et al. 2014, arXiv:1411.1415

Uhm, Z. L., & Zhang, B. 2014, arXiv:1411.0118

Virgili, F. J., Mundell, C. G., Pal'shin, V., et al. 2013, ApJ, 778, 54

Woods, E., & Loeb, A. 1995, ApJ, 453, 583

Wu, X. F., Dai, Z2010ApJ...725.1965L. G., Wang, X. Y., et al. 2006, 36th COSPAR Scientific Assembly, 36, 731

Zhang, B., Fan, Y. Z., Dyks, J., et al. 2006, ApJ, 642, 354

Zhang, B., & Mészáros, P. 2004, International Journal of Modern Physics A, 19, 2385

Zhang, B.-B., Liang, E.-W., & Zhang, B. 2007, ApJ, 666, 1002

Zhang, B.-B., Zhang, B., Liang, E.-W., & Wang, X.-Y. 2009, ApJ, 690, L10

Zhang, B.-B., Zhang, B., Murase, K., Connaughton, V., & Briggs, M. S. 2014, ApJ, 787, 66

Uhm, Z. L., & Zhang, B. 2015, ApJ, 808, 33

This preprint was prepared with the AAS LaTeX macros v5.2.

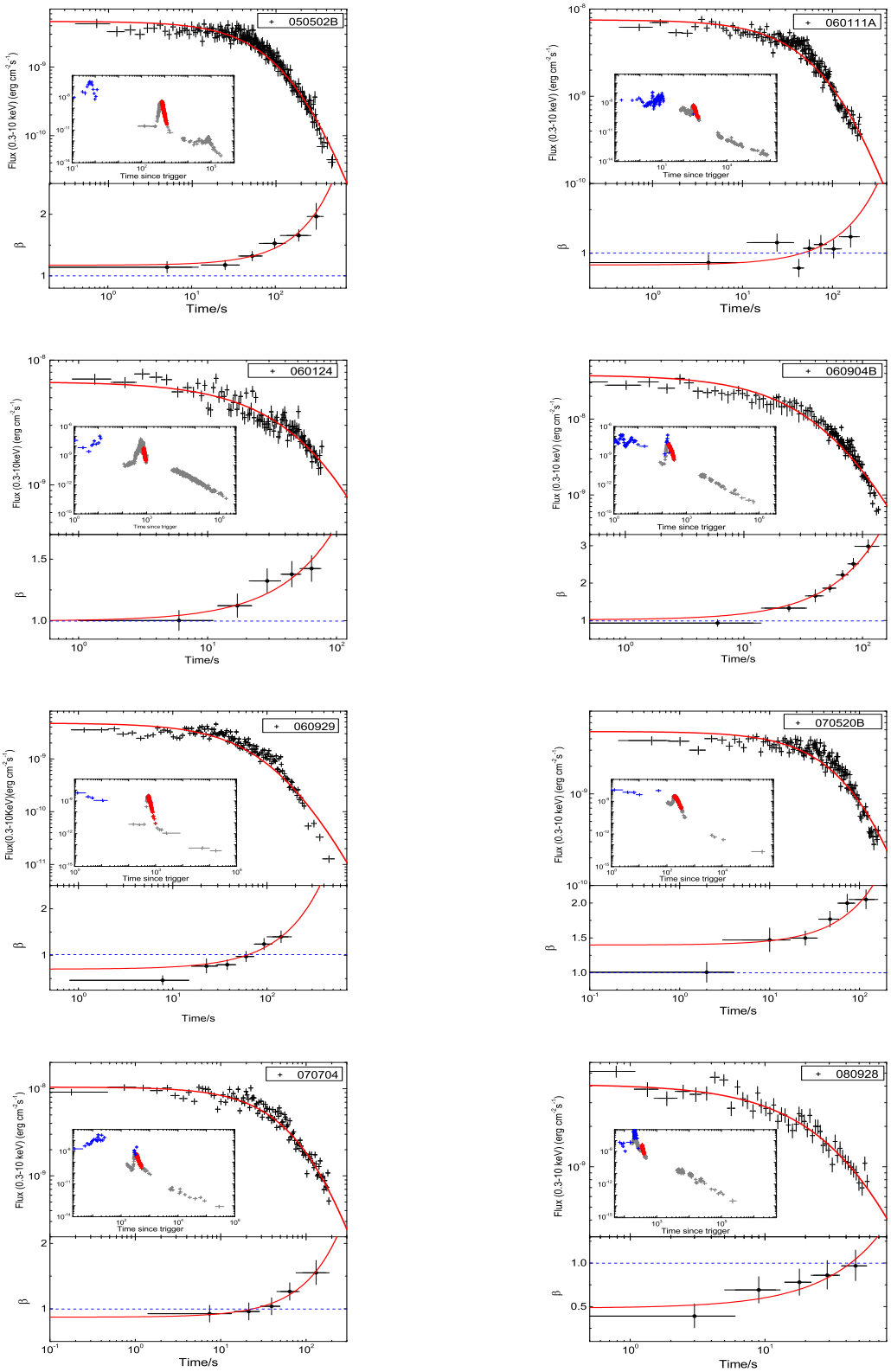

Fig. 1.— Lightcurves (upper part of each panel) and spectral index β evolution (lower part of each panel) of the steep decay segment in our selected 29 flares. The zero time is set to the peak time of the flares to timing the flare tails. Our joint fits are also shown with solid curves. The inset shows the light curve in $0.3-10$ keV of XRT observation (red and gray) and extrapolation based on BAT

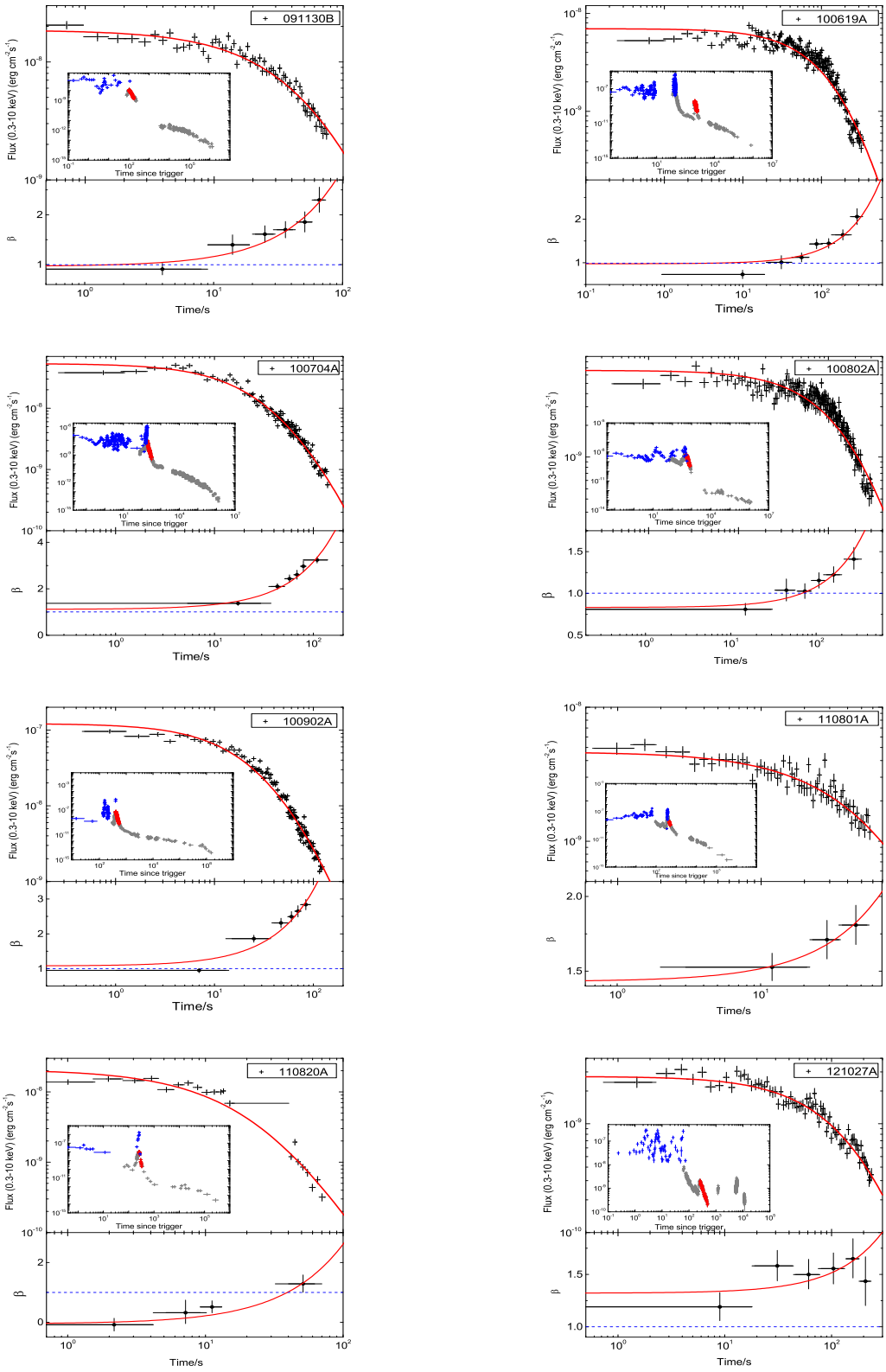

Fig. 1.— (Continued)

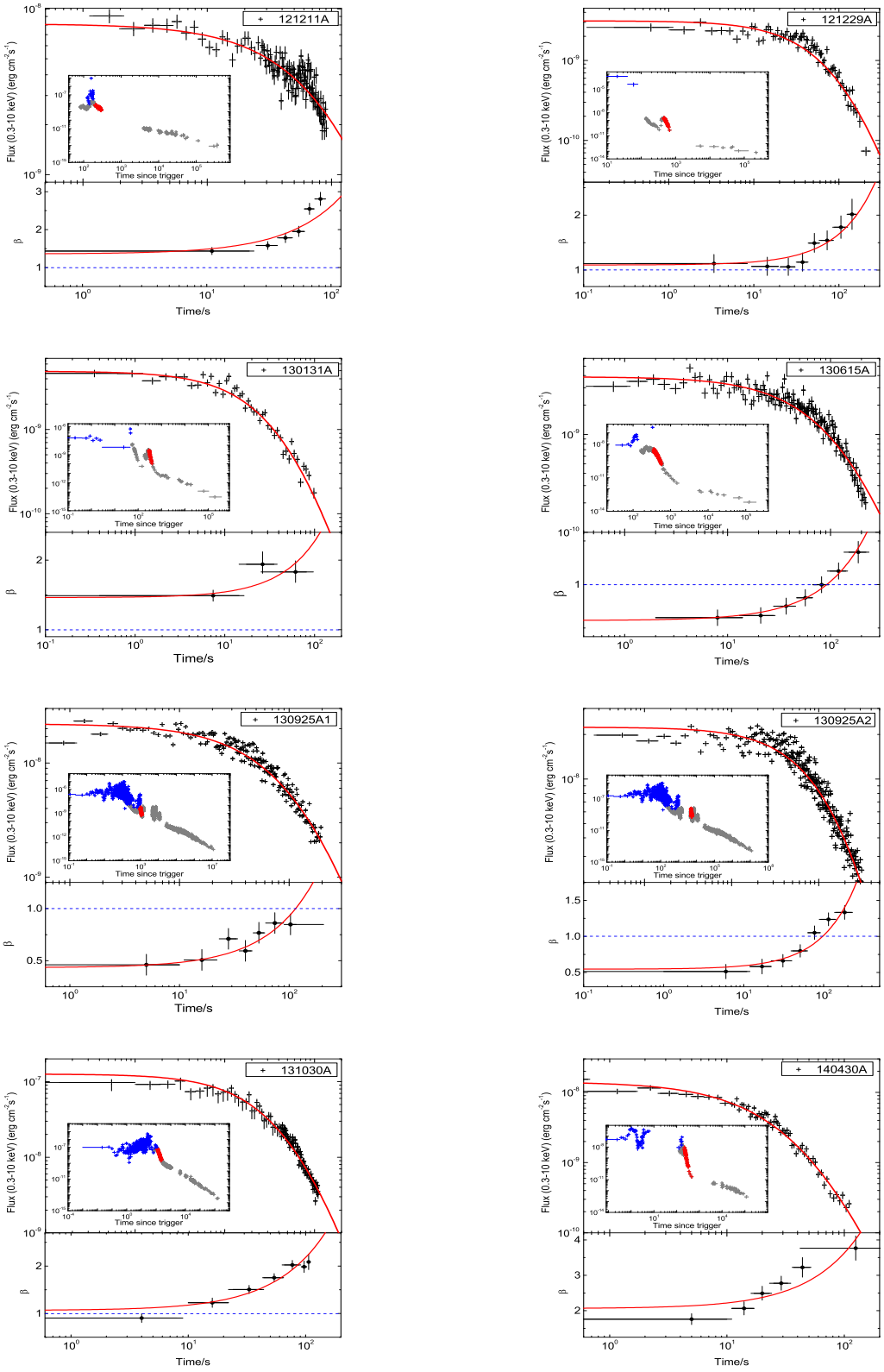

Fig. 1.— (Continued)

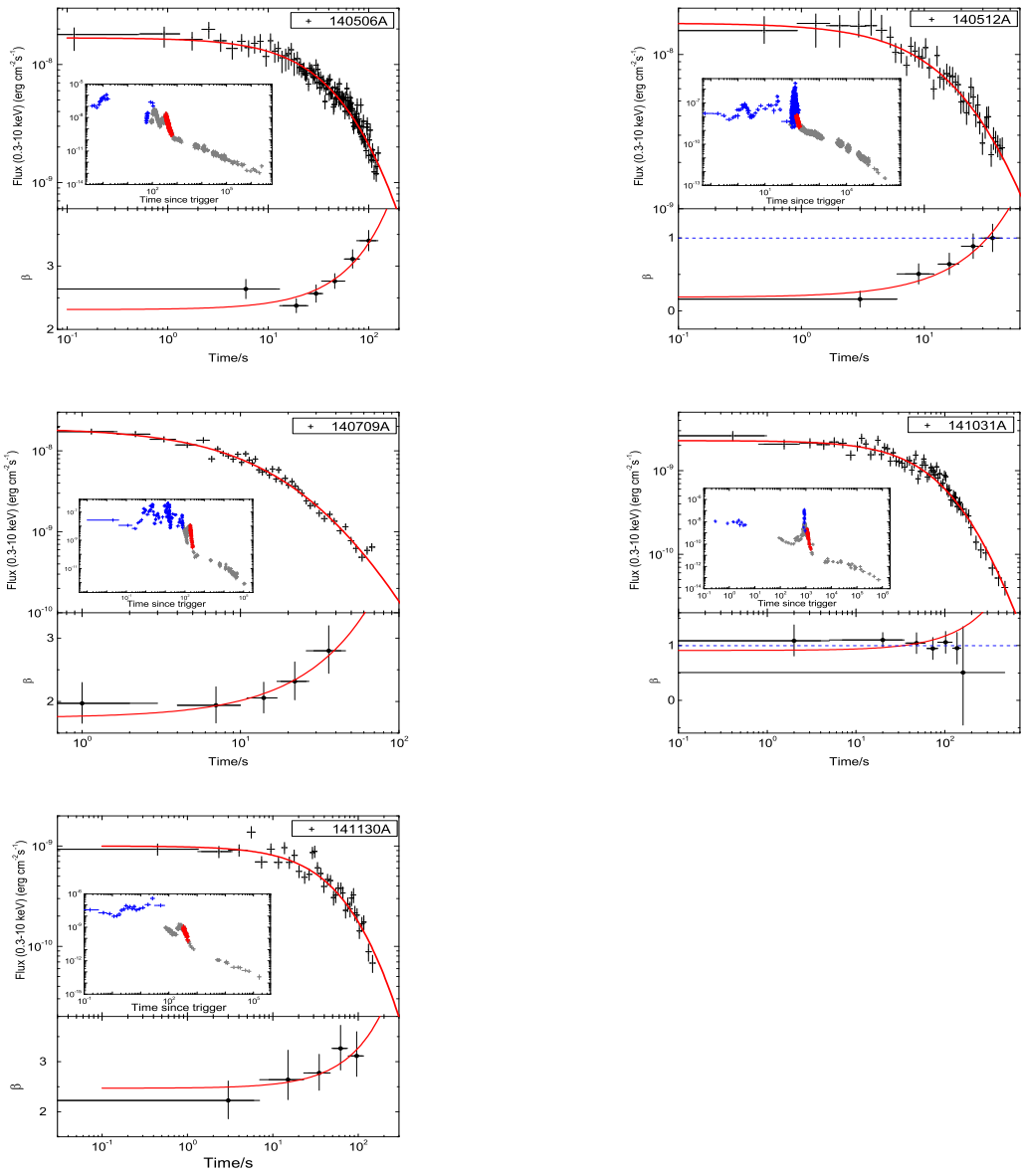

Fig. 1.— (Continued)

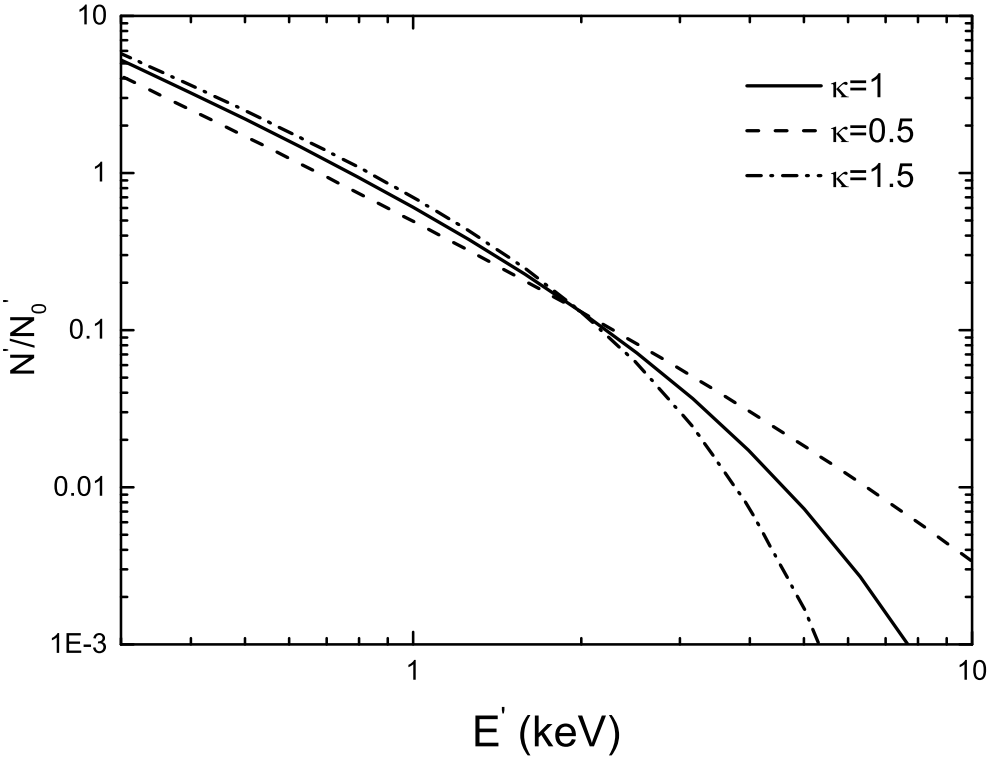

Fig. 2.— General Cut-off power spectral model (Eq. 4) in different deepness parameter κ.

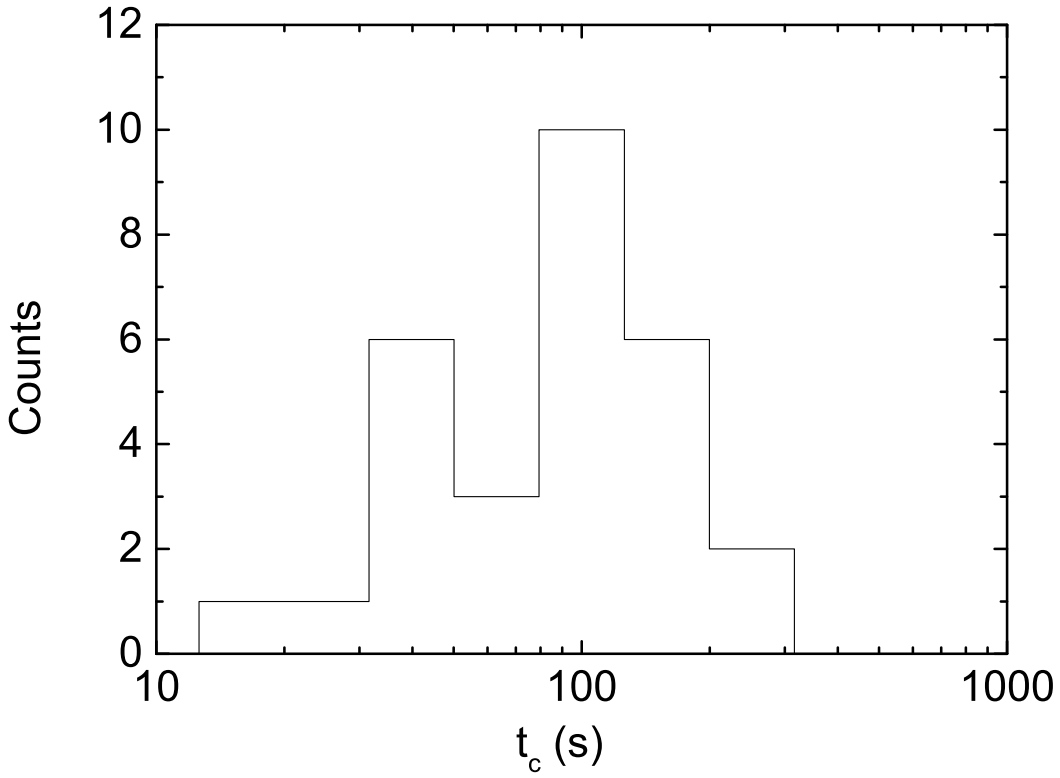

Fig. 3.— Distributions of t_c derived from our fits.

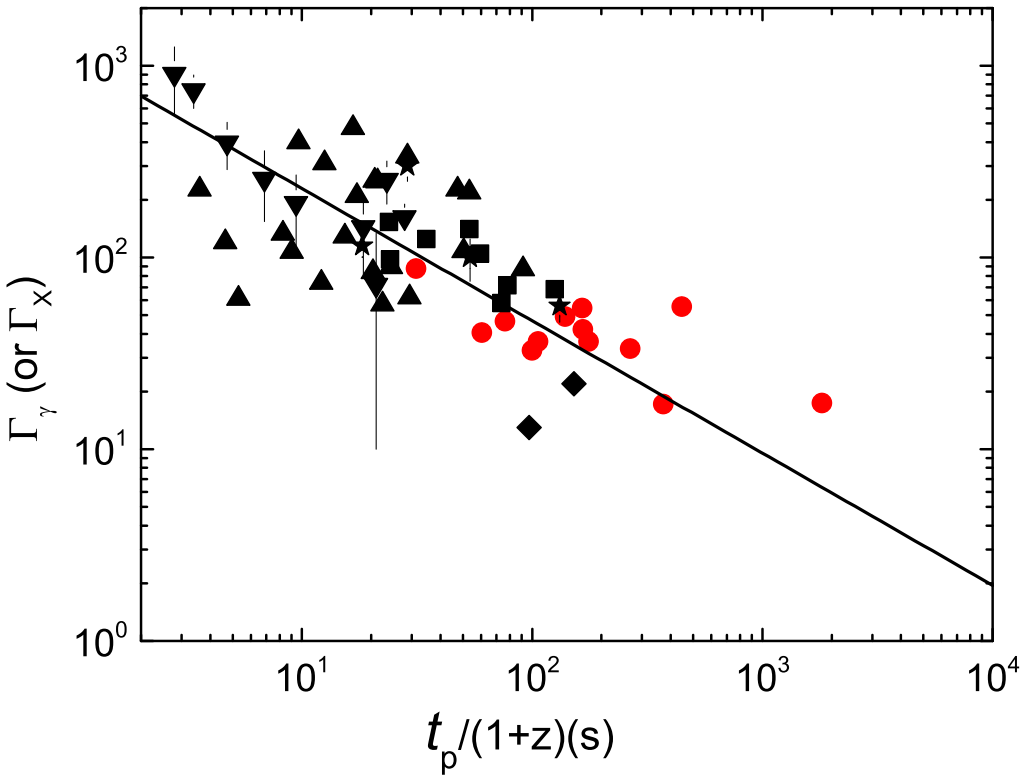

Fig. 4.— Lorentz factor (Γ_γ or $\Gamma_{\rm X}$) as a function of t_p for both the prompt gamma-rays and X-ray flares. The red dots are the X-ray flares in our sample. The symbols of "▲", "■", "★", "▼", and "♦" represent the data from Liang et al.(2013), Peng et al.(2014), Troja et al.(2014) (assuming the variation timescale of 0.1s), Tang et al.(2014), and Fan et al.(2005), respectively. The line is the regression line with the Spearman correlation analysis method.

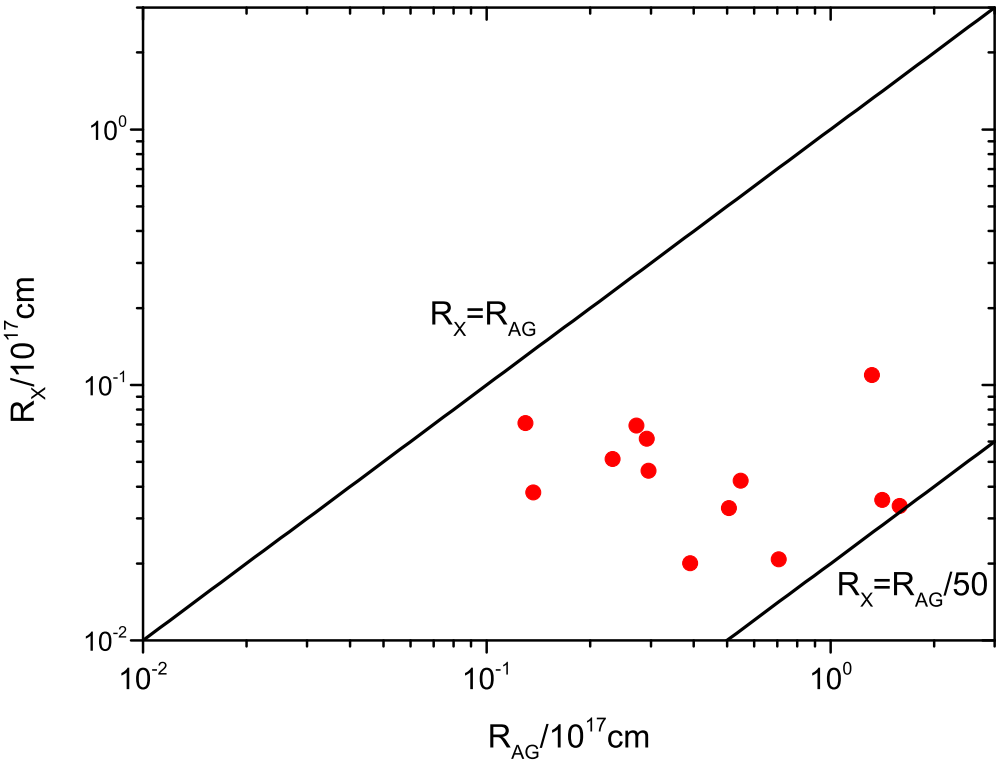

Fig. 5.— Comparison between the radii of the X-ray flare fireballs ($R_{\rm X}$) and the radii of the afterglow fireballs at the peak time of the flares ($R_{\rm AG}$). Lines of $R_{\rm X} = R_{\rm AG}$ and $R_{\rm X} = R_{\rm AG}/50$ are also marked.

Table 1. Results of time-resolved spectral analysis for the steep decay phases of the X-ray flares in our sample

GRB	interval (s)	mean time (s)	β	$N_{\rm H}^{\rm host}$ (10^{22} cm^{-2})	C_stat/bin
050502B	714 - 767	760	$1.14^{+0.09}_{-0.09}$	0.03	878/859
–	768 - 792	780	$1.17^{+0.08}_{-0.07}$	–	–
–	793 - 825	808	$1.32^{+0.08}_{-0.08}$	–	–
–	827 - 887	853	$1.53^{+0.08}_{-0.08}$	–	–
–	892 - 1021	945	$1.66^{+0.10}_{-0.09}$	–	–
–	1031 - 1130	1062	$1.96^{+0.22}_{-0.21}$	–	–
060111A	283 - 294	288	$0.89^{+0.09}_{-0.08}$	0.13	810/743
–	295 - 319	308	$1.12^{+0.10}_{-0.10}$	–	–
–	320 - 331	326	$0.83^{+0.10}_{-0.10}$	–	–
–	332 - 347	339	$1.06^{+0.10}_{-0.10}$	–	–
–	347 - 370	358	$1.10^{+0.11}_{-0.11}$	–	–
–	371 - 410	387	$1.05^{+0.11}_{-0.10}$	–	–
–	413 - 483	443	$1.19^{+0.12}_{-0.12}$	–	–
060124	761 - 771	766	$2.00^{+0.08}_{-0.08}$	0.13	630/623
–	772 - 782	777	$2.12^{+0.10}_{-0.09}$	–	–
–	782 - 797	789	$2.32^{+0.10}_{-0.10}$	–	–
–	798 - 813	805	$2.38^{+0.10}_{-0.10}$	–	–
–	814 - 836	824	$2.42^{+0.11}_{-0.10}$	–	–
060904B	172 - 184	178	$0.93^{+0.09}_{-0.09}$	0.49	692/645
–	187 - 220	196	$1.33^{+0.10}_{-0.10}$	–	–
–	207 - 252	212	$1.66^{+0.17}_{-0.16}$	–	–
–	219 - 278	225	$1.86^{+0.10}_{-0.10}$	–	–
–	233 - 308	240	$2.22^{+0.12}_{-0.12}$	–	–
–	249 - 340	256	$2.52^{+0.15}_{-0.14}$	–	–
–	268 - 396	284	$2.98^{+0.18}_{-0.17}$	–	–
060929	527 - 542	535	$0.46^{+0.10}_{-0.10}$	0.11	500/470
–	543 - 557	550	$0.77^{+0.16}_{-0.15}$	–	–
–	557 - 574	565	$0.80^{+0.11}_{-0.11}$	–	–
–	575 - 600	587	$0.97^{+0.11}_{-0.11}$	–	–
–	602 - 640	620	$1.24^{+0.12}_{-0.12}$	–	–
–	642 - 709	668	$1.40^{+0.13}_{-0.13}$	–	–
070520B	180 - 184	182	$1.01^{+0.15}_{-0.14}$	0.20	563/453
–	185 - 197	190	$1.47^{+0.17}_{-0.17}$	–	–
–	197 - 214	205	$1.50^{+0.10}_{-0.10}$	–	–
–	216 - 239	227	$1.77^{+0.11}_{-0.11}$	–	–
–	239 - 269	253	$2.00^{+0.13}_{-0.12}$	–	–
–	270 - 340	298	$2.05^{+0.14}_{-0.14}$	–	–

Table 1—Continued

GRB	interval (s)	mean time (s)	β	$N_{\rm H}^{\rm host}$ (10^{22} cm^{-2})	C_stat/bin
070704	338 - 350	344	$0.93^{+0.13}_{-0.13}$	0.32	977/924
–	351 - 365	358	$0.96^{+0.13}_{-0.13}$	–	–
–	366 - 386	376	$1.04^{+0.13}_{-0.13}$	–	–
–	387 - 420	401	$1.26^{+0.13}_{-0.13}$	–	–
–	428 - 523	468	$1.55^{+0.19}_{-0.18}$	–	–
080928	355 - 361	358	$0.39^{+0.14}_{-0.13}$	0.38	259/257
–	361 - 368	364	$0.69^{+0.15}_{-0.15}$	–	–
–	369 - 377	373	$0.78^{+0.15}_{-0.15}$	–	–
–	378 - 391	384	$0.86^{+0.17}_{-0.16}$	–	–
–	392 - 412	402	$0.97^{+0.18}_{-0.17}$	–	–
091130B	103 - 112	107	$0.91^{+0.12}_{-0.12}$	0.31	657/665
–	112 - 122	117	$1.40^{+0.20}_{-0.19}$	–	–
–	123 - 132	128	$1.61^{+0.17}_{-0.16}$	–	–
–	134 - 146	139	$1.70^{+0.17}_{-0.16}$	–	–
–	147 - 161	154	$1.85^{+0.21}_{-0.20}$	–	–
–	163 - 177	169	$2.30^{+0.26}_{-0.25}$	–	–
100619A	949 - 968	959	$0.73^{+0.10}_{-0.10}$	0.47	818/772
–	969 - 991	980	$1.01^{+0.16}_{-0.15}$	–	–
–	992 - 1019	1005	$1.12^{+0.10}_{-0.10}$	–	–
–	1020 - 1052	1036	$1.43^{+0.11}_{-0.11}$	–	–
–	1053 - 1097	1073	$1.44^{+0.11}_{-0.11}$	–	–
–	1100 - 1191	1137	$1.64^{+0.12}_{-0.12}$	–	–
–	1195 - 1286	1234	$2.06^{+0.18}_{-0.18}$	–	–
100704A	196 - 228	208	$1.37^{+0.07}_{-0.08}$	0.31	1064/820
–	228 - 242	234	$2.10^{+0.13}_{-0.12}$	–	–
–	242 - 254	248	$2.43^{+0.17}_{-0.16}$	–	–
–	255 - 264	259	$2.60^{+0.20}_{-0.19}$	–	–
–	265 - 275	270	$2.96^{+0.23}_{-0.23}$	–	–
–	270 - 330	300	$3.24^{+0.13}_{-0.13}$	–	–
100802A	507 - 538	522	$0.81^{+0.07}_{-0.07}$	0.03	995/826
–	541 - 564	552	$1.04^{+0.13}_{-0.13}$	–	–
–	567 - 594	581	$1.03^{+0.09}_{-0.09}$	–	–
–	598 - 635	615	$1.16^{+0.09}_{-0.09}$	–	–
–	640 - 707	668	$1.22^{+0.10}_{-0.09}$	–	–
–	719 - 818	784	$1.41^{+0.14}_{-0.12}$	–	–
100902A	418 - 431	424	$0.95^{+0.05}_{-0.07}$	–	–
–	432 - 454	442	$1.86^{+0.10}_{-0.10}$	–	–

Table 1—Continued

GRB	interval (s)	mean time (s)	β	$N_{\rm H}^{\rm host}$ (10^{22} cm^{-2})	C_stat/bin
–	457 - 473	464	$2.31^{+0.13}_{-0.14}$	–	–
–	473 - 482	477	$2.49^{+0.14}_{-0.15}$	–	–
–	482 - 492	487	$2.65^{+0.16}_{-0.16}$	–	–
–	493 - 511	501	$2.84^{+0.15}_{-0.15}$	–	–
110801A	453 - 472	462	$1.53^{+0.09}_{-0.09}$	–	1103/833
–	473 - 486	479	$1.71^{+0.13}_{-0.13}$	–	–
–	487 - 507	496	$1.81^{+0.13}_{-0.13}$	–	–
110820A	258 - 262	260	$-0.08^{+0.21}_{-0.21}$	–	181/157
–	262 - 267	265	$0.32^{+0.42}_{-0.36}$	–	–
–	267 - 271	269	$0.51^{+0.21}_{-0.20}$	–	–
–	298 - 328	309	$1.28^{+0.30}_{-0.28}$	–	–
121027A	259 - 277	268	$1.19^{+0.14}_{-0.13}$	1.33	338/322
–	278 - 303	290	$1.58^{+0.15}_{-0.14}$	–	–
–	305 - 337	320	$1.50^{+0.15}_{-0.14}$	–	–
–	339 - 392	363	$1.56^{+0.15}_{-0.15}$	–	–
–	397 - 441	418	$1.65^{+0.19}_{-0.18}$	–	–
–	446 - 494	467	$1.44^{+0.23}_{-0.23}$	–	–
121211A	182 - 203	192	$1.44^{+0.10}_{-0.10}$	1.20	1211/818
–	204 - 228	215	$1.58^{+0.11}_{-0.10}$	–	–
–	229 - 241	235	$1.78^{+0.13}_{-0.13}$	–	–
–	242 - 253	247	$1.95^{+0.14}_{-0.13}$	–	–
–	253 - 265	259	$2.55^{+0.15}_{-0.15}$	–	–
–	265 - 277	271	$2.81^{+0.18}_{-0.17}$	–	–
121229A	458 - 467	462	$1.12^{+0.17}_{-0.17}$	0.50	352/309
–	468 - 478	473	$1.07^{+0.17}_{-0.17}$	–	–
–	479 - 489	484	$1.06^{+0.16}_{-0.16}$	–	–
–	490 - 501	496	$1.14^{+0.17}_{-0.17}$	–	–
–	490 - 518	510	$1.49^{+0.18}_{-0.17}$	–	–
–	490 - 545	531	$1.54^{+0.18}_{-0.17}$	–	–
–	490 - 585	564	$1.78^{+0.21}_{-0.20}$	–	–
–	490 - 619	601	$2.01^{+0.28}_{-0.27}$	–	–
130131A	293 - 310	301	$1.49^{+0.08}_{-0.08}$	0.30	281/219
–	311 - 332	320	$1.94^{+0.18}_{-0.13}$	–	–
–	335 - 391	355	$1.83^{+0.16}_{-0.15}$	–	–
130615A	356 - 368	362	$0.62^{+0.09}_{-0.09}$	0.00	764/659
–	368 - 383	375	$0.64^{+0.09}_{-0.09}$	–	–
–	384 - 400	391	$0.75^{+0.09}_{-0.09}$	–	–

Table 1—Continued

GRB	interval (s)	mean time (s)	β	$N_{\rm H}^{\rm host}$ (10^{22} cm^{-2})	C_stat/bin
–	401 - 421	411	$0.85^{+0.09}_{-0.10}$	–	–
–	422 - 451	436	$1.00^{+0.09}_{-0.09}$	–	–
–	453 - 501	474	$1.15^{+0.09}_{-0.09}$	–	–
–	505 - 591	540	$1.37^{+0.12}_{-0.12}$	–	–
130925A1	997 - 1007	1002	$0.46^{+0.10}_{-0.10}$	1.59	874/862
–	1008 - 1019	1013	$0.51^{+0.10}_{-0.10}$	–	–
–	1020 - 1031	1025	$0.71^{+0.11}_{-0.11}$	–	–
–	1032 - 1043	1037	$0.59^{+0.12}_{-0.12}$	–	–
–	1044 - 1057	1050	$0.77^{+0.12}_{-0.12}$	–	–
–	1058 - 1086	1071	$0.86^{+0.10}_{-0.10}$	–	–
–	1087 - 1131	1107	$0.85^{+0.10}_{-0.10}$	–	–
130925A2	5020 - 5031	5026	$0.51^{+0.10}_{-0.10}$	1.59	1189/1218
–	5032 - 5042	5037	$0.58^{+0.10}_{-0.10}$	–	–
–	5043 - 5060	5051	$0.66^{+0.09}_{-0.09}$	–	–
–	5061 - 5083	5071	$0.80^{+0.09}_{-0.09}$	–	–
–	5084 - 5111	5097	$1.05^{+0.09}_{-0.09}$	–	–
–	5112 - 5162	5135	$1.24^{+0.09}_{-0.09}$	–	–
–	5163 - 5249	5203	$1.33^{+0.10}_{-0.10}$	–	–
131030A	116 - 125	120	$0.90^{+0.09}_{-0.09}$	0.61	907/769
–	126 - 138	132	$1.23^{+0.10}_{-0.10}$	–	–
–	140 - 160	149	$1.51^{+0.09}_{-0.09}$	–	–
–	160 - 181	170	$1.75^{+0.09}_{-0.08}$	–	–
–	182 - 207	193	$2.02^{+0.09}_{-0.09}$	–	–
–	208 - 218	213	$1.99^{+0.12}_{-0.12}$	–	–
–	219 - 225	222	$2.09^{+0.16}_{-0.16}$	–	–
140430A	222 - 233	227	$1.76^{+0.16}_{-0.15}$	0.91	319/298
–	233 - 239	236	$2.06^{+0.19}_{-0.18}$	–	–
–	239 - 246	242	$2.49^{+0.20}_{-0.19}$	–	–
–	247 - 257	251	$2.78^{+0.20}_{-0.19}$	–	–
–	259 - 274	266	$3.22^{+0.28}_{-0.27}$	–	–
140506A	359 - 372	365	$2.64^{+0.15}_{-0.15}$	0.64	772/567
–	373 - 384	378	$2.38^{+0.11}_{-0.11}$	–	–
–	385 - 394	389	$2.57^{+0.14}_{-0.14}$	–	–
–	395 - 417	405	$2.76^{+0.12}_{-0.12}$	–	–
–	417 - 440	428	$3.11^{+0.15}_{-0.15}$	–	–
–	441 - 483	459	$3.40^{+0.16}_{-0.16}$	–	–
140512A	144 - 150	147	$0.16^{+0.11}_{-0.11}$	0.20	346/304

Table 1—Continued

GRB	interval (s)	mean time (s)	β	$N_{\rm H}^{\rm host}$ (10^{22} cm^{-2})	C_stat/bin
–	151 - 156	153	$0.51^{+0.14}_{-0.14}$	–	–
–	157 - 163	160	$0.64^{+0.15}_{-0.15}$	–	–
–	164 - 173	169	$0.88^{+0.17}_{-0.17}$	–	–
–	175 - 187	180	$1.00^{+0.19}_{-0.19}$	–	–
140709A	189 - 192	190	$1.97^{+0.33}_{-0.32}$	0.28	187/187
–	193 - 199	196	$1.94^{+0.29}_{-0.28}$	–	–
–	200 - 206	203	$2.05^{+0.25}_{-0.24}$	–	–
–	207 - 216	211	$2.32^{+0.31}_{-0.29}$	–	–
–	218 - 235	225	$2.80^{+0.40}_{-0.36}$	–	–
141031A	1104 - 1109	1106	$1.09^{+0.29}_{-0.28}$	0.12	263/220
–	1111 - 1139	1124	$1.10^{+0.13}_{-0.13}$	–	–
–	1141 - 1164	1152	$1.05^{+0.19}_{-0.19}$	–	–
–	1167 - 1187	1177	$0.95^{+0.20}_{-0.20}$	–	–
–	1191 - 1225	1206	$1.06^{+0.20}_{-0.20}$	–	–
–	1229 - 1256	1241	$0.95^{+0.29}_{-0.29}$	–	–
–	1262 - 1578	1264	$0.51^{+0.84}_{-0.96}$	–	–
141130A	329 - 336	332	$2.22^{+0.39}_{-0.36}$	0.20	110/126
–	338 - 352	344	$2.64^{+0.59}_{-0.40}$	–	–
–	355 - 376	364	$2.77^{+0.37}_{-0.35}$	–	–
–	380 - 404	391	$3.26^{+0.46}_{-0.43}$	–	–
–	409 - 445	425	$3.11^{+0.48}_{-0.41}$	–	–

Table 2. Curvature effect model fits to the evolution behaviors of flux and spectral index in the steep decay phase of the X-ray flares in our sample.

GRB	$F_{E,0}$ ($10^{-9}\mathrm{erg}\cdot\mathrm{cm}^{-2}\cdot\mathrm{s}^{-1}\cdot\mathrm{keV}^{-1}$)	$\hat{\beta}$	$E_{c,0}$ (keV)	t_c (s)	χ^2/dof
050502B	1.77 ± 0.05	1.69 ± 0.04	5.72 ± 0.24	171.71 ± 3.38	1.32
060111A	2.28 ± 0.07	1.51 ± 0.04	7.76 ± 0.24	121.13 ± 2.17	3.03
60124	2.74 ± 0.16	1.04 ± 0.06	2.90 ± 0.12	123.25 ± 4.58	1.80
060904B	16.46 ± 0.72	0.93 ± 0.18	2.54 ± 0.24	65.39 ± 1.41	3.98
60929	1.37 ± 0.07	1.10 ± 0.06	4.62 ± 0.16	121.01 ± 2.00	8.31
070520B	2.33 ± 0.12	1.56 ± 0.06	3.28 ± 0.10	138.59 ± 2.71	3.76
70704	3.58 ± 0.19	1.17 ± 0.06	3.96 ± 0.12	129.90 ± 2.39	4.42
80928	1.03 ± 0.08	0.68 ± 0.10	3.42 ± 0.26	67.73 ± 3.13	1.36
091130B	9.05 ± 0.52	0.28 ± 0.53	1.64 ± 0.46	86.13 ± 2.34	2.09
100619A	2.73 ± 0.10	1.12 ± 0.05	3.22 ± 0.06	253.92 ± 3.21	6.51
100704A	24.07 ± 0.99	1.11 ± 0.16	2.74 ± 0.20	49.50 ± 1.13	3.32
100802A	2.14 ± 0.07	1.23 ± 0.05	4.62 ± 0.16	242.57 ± 4.42	2.93
100902A	52.50 ± 1.65	1.12 ± 0.15	2.88 ± 0.24	43.86 ± 0.76	6.64
110801A	2.40 ± 0.41	1.46 ± 0.08	2.84 ± 0.14	113.27 ± 5.56	1.24
110820A	2.59 ± 0.56	0.31 ± 0.28	4.32 ± 1.08	23.98 ± 1.19	6.01
121027A	1.06 ± 0.14	1.81 ± 0.05	5.38 ± 0.14	264.63 ± 8.92	1.64
121211A	5.96 ± 0.23	0.10 ± 0.08	1.22 ± 0.02	179.31 ± 6.44	2.22
121229A	1.26 ± 0.06	1.35 ± 0.07	3.74 ± 0.16	130.88 ± 3.18	3.69
130131A	2.02 ± 0.16	2.00 ± 0.05	5.92 ± 0.20	57.87 ± 1.75	3.24
130615A	1.05 ± 0.04	0.88 ± 0.06	3.94 ± 0.16	156.82 ± 3.20	2.34
130925A1	5.18 ± 0.14	0.66 ± 0.04	3.56 ± 0.04	157.63 ± 1.35	13.79
130925A2	6.61 ± 0.15	0.39 ± 0.04	2.38 ± 0.02	247.51 ± 1.45	18.70
131030A	47.79 ± 1.86	1.46 ± 0.14	4.54 ± 0.54	54.61 ± 1.40	1.76
140430A	7.25 ± 0.64	2.25 ± 0.07	3.42 ± 0.12	51.52 ± 1.36	2.48
140506A	11.43 ± 1.38	1.96 ± 0.97	2.04 ± 1.14	129.17 ± 21.95	1.21
140512A	3.11 ± 0.26	0.10 ± 0.54	2.54 ± 0.12	43.60 ± 2.83	0.88
140709A	10.43 ± 1.76	1.82 ± 0.11	3.00 ± 0.12	33.55 ± 1.16	1.90
141031A	0.73 ± 0.05	1.44 ± 0.07	5.86 ± 0.16	180.30 ± 6.71	1.39
141130A	0.66 ± 0.35	2.11 ± 0.17	2.04 ± 0.14	167.56 ± 10.17	1.78

Table 3: $R_{\rm X}$ and $\Gamma_{\rm X}$ for flares with known redshift

GRB	z	α	β	E_p (keV)	model	χ^2/dof	F_p ($10^{-9}{\rm erg\cdot cm^{-2}\cdot s^{-1}}$)	$L_{\rm X,p}$ ($10^{48}{\rm erg\cdot s^{-1}}$)	$\Gamma_{\rm X}$	$R_{\rm X}$ ($10^{15}{\rm cm}$)
060124	2.297	$2^{+0.08}_{-0.08}$	–	–	power-law	1.01	6.78 ± 0.16	286 ± 6.74	55.60 ± 3.43	6.93 ± 0.89
060904B	0.703	$0.93^{+0.09}_{-0.09}$	–	–	band	1.08	50.24 ± 1.1	113 ± 2.47	40.54 ± 2.89	3.79 ± 0.55
080928	1.692	$0.39^{+0.13}_{-0.14}$	–	–	power-law	1.01	4.17 ± 0.13	82.6 ± 2.58	36.46 ± 2.73	2.01 ± 0.32
110801A	1.858	$2.61^{+0.11}_{-0.10}$	–	–	power-law	0.99	5.07 ± 0.13	127 ± 3.25	42.15 ± 2.96	4.23 ± 0.63
121027A	1.773	$1.19^{+0.14}_{-0.13}$	–	–	power-law	1.05	2.72 ± 0.06	60.5 ± 1.33	32.79 ± 2.56	6.16 ± 0.98
121211A	1.023	$-0.91^{+0.38}_{-0.51}$	$-2.49^{+0.11}_{-0.27}$	2.02 ± 1.71	band	1.98	14.57 ± 0.22	82.8 ± 1.25	36.49 ± 2.71	7.08 ± 1.08
121229A	2.707	$1.12^{+0.17}_{-0.17}$	–	–	power-law	1.14	3.19 ± 0.06	200 ± 3.76	49.24 ± 3.21	5.14 ± 0.68
130925A1	0.347	$0.46^{+0.10}_{-0.10}$	–	–	power-law	1.01	22 ± 0.11	9.1 ± 0.05	17.19 ± 1.71	2.08 ± 0.41
130925A2	0.347	$0.51^{+0.10}_{-0.10}$	–	–	power-law	0.98	23 ± 0.1	9.5 ± 0.04	17.46 ± 1.73	3.36 ± 0.67
131030A	1.293	$-0.91^{+0.46}_{-0.34}$	$-3.19^{+0.24}_{-0.39}$	2.13 ± 2.04	band	1.15	106.67 ± 3.81	1080 ± 38.8	87.51 ± 4.45	10.94 ± 1.15
140430A	1.6	$2.75^{+0.14}_{-0.14}$	–	–	power-law	0.96	15.71 ± 0.35	271 ± 6.04	54.61 ± 3.40	3.55 ± 0.45
140506A	0.889	$2.64^{+0.15}_{-0.15}$	–	–	power-law	1.36	16.1 ± 0.48	64.6 ± 1.93	33.53 ± 2.60	4.61 ± 1.06
140512A	0.725	$-0.42^{+0.73}_{-0.50}$	$-1.61^{+0.05}_{-0.07}$	5.14 ± 4.51	band	1.45	70.14 ± 4.64	170 ± 11.3	46.60 ± 3.27	3.29 ± 0.51